RSC Advances

This is an *Accepted Manuscript*, which has been through the Royal Society of Chemistry peer review process and has been accepted for publication.

Accepted Manuscripts are published online shortly after acceptance, before technical editing, formatting and proof reading. Using this free service, authors can make their results available to the community, in citable form, before we publish the edited article. This *Accepted Manuscript* will be replaced by the edited, formatted and paginated article as soon as this is available.

You can find more information about *Accepted Manuscripts* in the **Information for Authors**.

Please note that technical editing may introduce minor changes to the text and/or graphics, which may alter content. The journal's standard **Terms & Conditions** and the **Ethical guidelines** still apply. In no event shall the Royal Society of Chemistry be held responsible for any errors or omissions in this *Accepted Manuscript* or any consequences arising from the use of any information it contains.

Advanced Materials

ARTICLE

Nanostructured oxyhydroxide niobium (NbO₂OH) as UV radiation protector for polypropylene

Samara D. Souza[a], Iaci M. Pereira[b], Ana Pacheli H. Rodrigues[c], Luiz C. A. Oliveira[c], Tulio P. Boaventura[d], Alexandre R. Souza[a], Rodrigo L. Oréfice[d], Patrícia S. O. Patrício[a*]

In this study a novel approach for improving the photo-stabilization of polymers by incorporation of nanoparticles of a new niobium compound is reported. For the first time, this approach uses the electronic properties of niobium oxyhydroxide to absorb UV light efficiently to avoid the decomposition of the polymers. The innovative results of this work consist of preparing nanoparticles of niobium oxyhydroxide and its modification by treatment with hydrogen peroxide to alter their ability to absorb radiation and act as photo-stabilizer for preventing polypropylene degradation. Synchrotron radiation was employed: (i) to explore the niobium nanoparticle form and (ii) to investigate the macromolecular structure of neat PP and PP/Nb compounds before and after degradation. The results from this research study used FTIR-ATR, DSC and microscopies, as TEM, SEM and OM, indicate that the incorporation of niobium oxyhydroxide nanoparticles into the PP matrix provide stability against the action of ultraviolet radiation.

1. Introduction

The properties of polypropylene (PP) are well-known and have been extensively investigated due to its wide applications in industrial and consumer products, medical products, packaging, automotive and electronic appliances. In addition to its excellent mechanical properties, resistance to chemicals and easy processing. However, this polymer exhibits low resistance to photo-oxidative degradation after prolonged exposure to weather. Solar light and other high-energy radiation are among the main causes of polymer degradation. The photochemical behavior of PP based materials is important because durability is a key factor for outdoor applications[1]. Polymeric photo-degradation can cause premature failure of the polymer during operation, which is primarily due to the appearance of surface cracks[2]. The study of polymer degradation and stabilization is important to lengthen the service life of the product[3-7]. In recent years, the economic importance of PP along with the development of nanotechnology renewed investigative efforts of the degradation mechanisms and photo-degradation[8-12].

The oxidation mechanism of PP is initiated photochemically by the oxidation of the tertiary carbon atoms, which induces the formation of tertiary hydroperoxide radical[5]. These radicals are photo-unstable[4] resulting in autocatalytic degradation reactions. The initiation step involves the formation of an alkyl radical due to the homolytic scission of a C-H bond, and this radical reacts with molecular oxygen dissolved in the polymer to yield peroxide radical. In the propagation and termination steps, the O-O bonds of the hydroperoxides, which have a low bond energy (190 kJ mol⁻¹), undergo homolytic scission to produce a hydroxyl and an alkoxyl radical[5]. Prior to the termination step, some reactions involving rearrangements occur, which yield different radical species that recombine to terminate the reaction. The products can include compounds containing hydroxyl or carbonyl groups.

Photo-stabilizers are categorized according to their mechanism of action. They can usually deactivate excited species, which can catalyze the decomposition of hydroperoxides, and compounds that can react with free radicals to interrupt degradative chain processes, such hindered amine light stabilizers (HALS)[8]. On the other hand, inorganic particles, such ZnO[12] and organic UV screeners, such as substituted benzophenone and benzotriazole have been employed to block UV irradiation photo-stabilizing PP. However, these organic UV screeners degrade and are subject to migration, which limits their usefulness and often necessitate increased loadings[13]. Carbon black is commonly used to photo-stabilize PP by acting as an absorption filter of UV radiation. In addition, carbon black acts as a scavenger of free radical deactivating excited species. However, the difficulty of dispersing it into the polymer matrix becomes a drawback to its use as UV screeners.

The materials from niobium may be modified to absorb radiation in the visible and ultraviolet region. Niobium oxide and oxyhydroxide can be used as semiconductors for use in photocatalytic reactions[14, 15] to treat contaminated effluent or

a. Centro Federal de Educação Tecnológica de Minas Gerais. Av. Amazonas, 5253, Nova Suiça, Belo Horizonte, MG. CEP 30421-169, Brazil.
b. Centro Tecnológico do Exército, Av. Américas, 28705, Guaratiba, Rio de Janeiro, RJ. CEP 23020-470, Brazil.
c. Departamento de Química and d. Departamento de Engenharia Metalúrgica e de Materiais, Universidade Federal de Minas Gerais. Av. Antônio Carlos, 6627, Pampulha, Belo Horizonte, MG. CEP 31270-901, Brazil.

even as radiation-absorbing filters aimed technological applications. Besides the excellent properties photo-absorbing, Brazil has large niobium ore reserves, which makes the development of great interest.

The current study investigated the novel photo-stabilization of PP using nanoparticles and particles of niobium oxyhydroxide into the polymer matrix. Our group has developed routes to modify the surface of the niobium oxyhydroxide nanoparticles: (i) by a treatment with hydrogen peroxide to alter its light absorption capacity[16] and generating amphiphilic niobium oxyhydroxide modified with a surfactant[17]. These modifications were essential to allow efficient absorption of UV radiation while preserving the integrity of the polymer. Moreover, the SAXS technique has been used to investigated the nanostructure of niobium compounds and PP/niobium compounds before and after UV photo-degradation.

2. Experimental

PP with a melt flow index of 22 g/10 min was supplied in the form of pellets by Borealis S.A. The nanoparticles of niobium oxyhydroxide were prepared by treating 0.26 M $NH_4[NbO(C_2O_4)_2(H_2O)].(H_2O)_n$ with 1 M NH_4OH (14.0 mL) followed by heating at 60 °C for 72 h NbO_2OH. This material was used as a precursor for the preparation of NbO_2OH/H_2O_2, which was obtained by treating NbO_2OH (300 mg) with 30% aqueous H_2O_2 (4 mL) in H_2O (80 mL) for 30 min. Then, the yellow solid was filtered, washed with distilled water, and dried at 60 °C for 12 h.

After, the surfactant compound cetyltrimethylammonium bromide (CTAB, 4.47 mmol, Vetec) was added to a suspension of NbO_2OH/H_2O_2 in H_2O, and the mixture was refluxed for 4 h to prepare the amphiphilic hybrid material NbO_2OH/amp. The resulting catalyst (yellow powder) was filtered, washed with water and dried at 60 °C.

The reagents, PP and loadings, were mixed together in a torque rheometer (Haake Poly Drive Mixer manufactured by Thermo Fischer Scientific) at 180 °C with a rotor speed of 35 rpm for 5 minutes. All of the samples contain 1 wt.% of the niobium compound. Films were obtained using the conventional hot-press method at 180°C for 5 minutes under 2 MPa of pressure.

An UV accelerated weathering test was performed using an EQUV Equilam equipment. Emitted light with a maximum intensity at a wavelength of 340 nm according to ASTM G154 was employed in the tests. The samples were subjected to alternating cycles with one lamp on at 70 °C for 8 hours and another lamp off with condensation activated at 50 °C for 4 hours, and the exposure times used of 5 and 10 days.

The morphological study of the composite and PP was carried out with a JEOL model 6360LV scanning electron microscope (SEM) operating at 15 kV with backscattered electrons. The samples were immersed in liquid nitrogen and broken. Moreover, the morphological study was carried out with a Tecnai G2-20 Super Twin FEI-200 kV transmission electron microscope (TEM). Surface cracking patterns for the UV

irradiation treated samples were observed by using an optical microscope (Leica DM 2500).

Synchrotron radiation was employed: (i) to explore the niobium nanoparticle form and (ii) to investigate the macromolecular structure of neat PP and PP/Nb composites before and after degradation. The niobium compound nanoparticle experiments were performed using a sample holder for solid. For measurement, a thin layer of powder samples was maintained onto the surface of a single Kapton tape. The scattering intensity was registered using a MAR-165 detector (165 mm diameter; 2048 x 2048 pixels) for SAXS. The sample-detector distance used during the measurements was 570 mm. To investigate the polymeric films nanostructure, the MAR-165 detector was employed, as well the sample holder for films placed at two different sample-detector distances. The distances used were: 1981 mm (Distance A) and 570 mm (Distance B). Additionally, to investigate NbO_2OH/H_2O_2 polymeric films nanostructure, the Dectris − Pilatus Multi − 3 stacked modules detector (84 x 107 mm; 487 x 619 pixels) was employed. For this experiment, the sample-detector distance used during the measurement was 3025 mm. The SAXS experiments were performed using the beam line of the National Synchrotron Light Laboratory (LNLS, Campinas, Brazil). The monochromatized wavelength used was $\lambda = 1.55$ Å. The data were corrected: for the parasitic scattering intensity produced by the collimating slits, for the non-constant sensitivity of the position sensitive X-ray detector, for the time varying intensity of the direct synchrotron beam and for the differences in sample thickness.

Differential scanning calorimetry (DSC) measurements were performed with the Seiko-sll nanotchnology-inc 7020 model Exaltar equipment in an inert atmosphere. The procedure for this measurement involved a first run scanning environment up to 190 °C followed by cooling to -20 °C and a second run to 200 °C at a heating rate of 20 °C/min.

The spectra infrared (FTIR-ATR) were obtained for all materials studied including pure PP and composite PP/Niobium compounds before and after UV exposure. Fourier transform infrared (FTIR) measurements were performed with a Shimadzu Prestige 21 spectrophotometer with a horizontal attenuated reflection (ATR) accessory in the region from 4000 to 400 cm^{-1} using the Krs-5 crystal with a scan number 60. The exposed surface of the samples was characterized. Characteristic PP bands were identified in the spectra of all of the materials. The ratio of the area under the doublet at 1720 and 1168 cm^{-1} from the PP and PP/Nb compounds was calculated to determine the carbonyl index. The carbonyl index was obtained using the ratio of the area under the bands located at 1168 cm[-1](A_{1168}) and 1720 cm^{-1} (A_{1720}) and eq. 1:

$$CI = 100 \text{ x } \left(\frac{A_{1720}}{A_{1720+1168}}\right) \qquad \text{(eq. 1)}$$
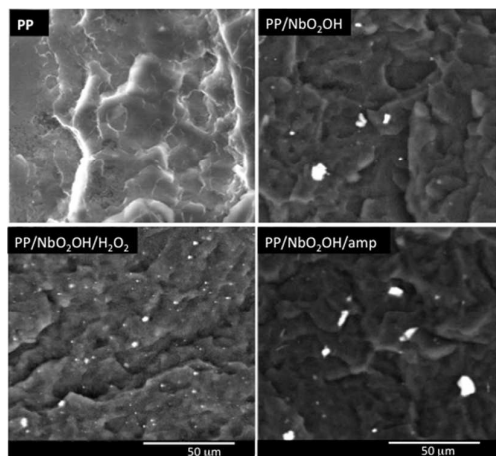
Figure 1. SEM micrograph of pure PP and the PP/NbO$_2$OH, PP/NbO$_2$OH/H$_2$O$_2$ and PP/NbO$_2$OH/amp.
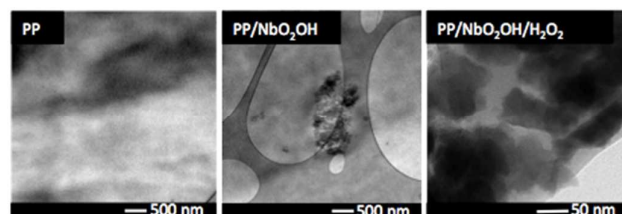
Figure 2. TEM image of pure PP and PP/niobium compounds: PP/NbO$_2$OH, and NbO$_2$OH/H$_2$O$_2$ in different magnification.

3. Results and discussion

3.1- Morphologic characterization

The dispersion state of the niobium oxyhydroxide in the PP matrix of the unexposed samples was investigated using a SEM (Figure 1). Figure 1 (a) shows the typical cryogenic fracture of PP, and Figures 1 (b), (c) and (d) show the cryogenic fracture of the PP/Nb compounds. The lighter domains, which are shown in Figures 1 (b), (c) and (d), represent the inorganic phase distributed in the polymeric matrix. Some particles tended to aggregate leading to domains with different sizes, as observed in the PP/NbO$_2$OH and PP/NbO$_2$OH/amp.

The SEM images indicate that there was a significant size reduction of the inorganic phases observed in the PP/NbO$_2$OH/H$_2$O$_2$, which led to a better dispersion of the particles in the polymeric matrix. This difference is due to the treatment of niobium oxyhydroxide with hydrogen peroxide, which is capable of promoting the breakage of the particles. The average size of the NbO$_2$OH/H$_2$O$_2$ aggregation is approximately 2.5 μm, as shown by SEM. However, the size of a single nanoparticle of niobium compounds is less than 100 nm, as revealed by TEM, Figure 2 (c). The dark regions observed in the Figures 2 (b) and 2 (c), TEM image of nanocomposite were considered nanoparticles agglomerated. This was not observed in the image for the PP sample (Figure 2(a)). In the Oliveira *et al.* used TEM image to show the nanosize of niobium compound in this kind of synthesis [17]. The

influence of nanoparticles in the polymer nanostructure was investigated by synchrotron small angle X-ray (SAXS).
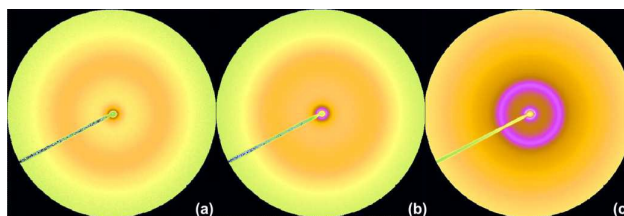
Figure 3 – SAXS 2D patterns of (a) NbO$_2$OH/H$_2$O$_2$, (b) NbO$_2$OH and (c) NbO$_2$OH/amp.
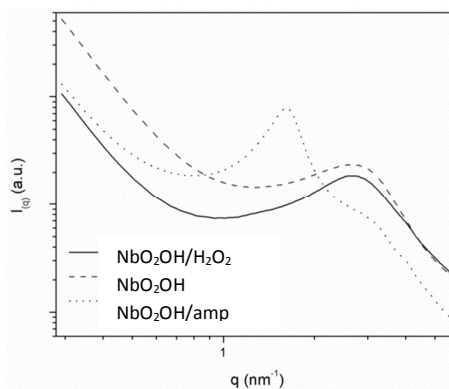
Figure 4 – SAXS scattering intensity of NbO$_2$, NbO$_2$OH/H$_2$O$_2$ and NbO$_2$OH/amp.
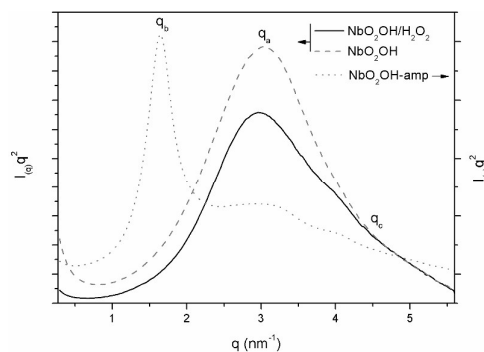
Figure 5 – Lorentz corrected plot of NbO$_2$, NbO$_2$OH/H$_2$O$_2$ and NbO$_2$OH/amp.

3.2- Synchrotron small angle X-ray scattering (SAXS)

3.2.1- The niobium nanoparticle form

Figure 3 illustrates SAXS patterns from the niobium nanoparticle. The scattering technique was employed to investigate the niobium nanocomposite shape, surface and compaction. Figure 4 presents the scattering intensity, *I(q),* as a function of the scattering vector **q**. Where **$q=(4\pi/\lambda)sin\theta$, θ** being half the scattering angle.

Figures 4 scattering data were elaborated with respect to the Lorentz corrected plot and the Porod's plot. The Lorentz corrected plot, Figure 5, was applied to assess the conformational of the particle. The Porod's plot, Figure 6, was used to describe de particle surface.The plots presented at Figure 5 are typical of organized structures. The symmetric maxima observed at NbO$_2$OH, $q_a = 3.023$ nm^{-1}, and at

NbO$_2$OH/H$_2$O$_2$, $q_a = 2.872$ nm^{-1}, curves suggest the existence of small spheroid like particles. As observed, the peak position of NbO$_2$OH/H$_2$O$_2$ moves to slightly smaller **q** values indicating an small increment in the structure size of NbO$_2$OH[18]. NbO$_2$OH/H$_2$O$_2$ is formed by different hydroxyl groups attached at NbO$_2$ surface.
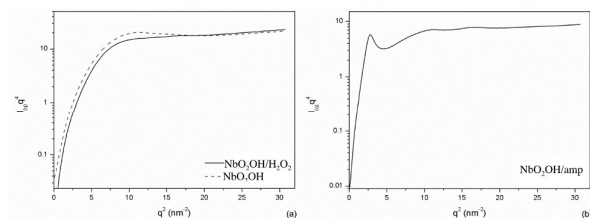
Figure 6 – Porod's plot of (a) NbO$_2$OH, NbO$_2$OH/H$_2$O$_2$ and (b) NbO$_2$OH/amp.

The O–H surface groups increase nanoparticle size without altering significantly the particle size. The asymmetric maximum presented on NbO$_2$OH/amp curve and the second-order peak presented as a 'bump' at larger q-values suggests elongated lamellar structure[18, 19]. At NbO$_2$OH/amp, the presence of the surfactant molecule extends the nanoparticle alowing the nanocompound to reorganize in the new shape.

At Figure 5 the niobium compound plots shows: a well defined bump around $q_a = 2.9$ nm^{-1}, attributed to NbO$_2$OH particles, an overlaid bump around $q_c = 4.0$ nm^{-1}, attributed to O–H surface groups and, observed at NbO$_2$OH/amp, a defined peak at $q_c = 1.658$ nm^{-1} attributed to the surfactant molecule. The contribution of each group were separated according to a deconvolution procedure[20, 21] to obtain the Porod invariant, ₋Q_{inv} is Porod invariant, Equation 2:

$$Q_{inv} = \int_0^\infty q^2 I_{(q)} dq \quad \text{(eq. 2)}$$

Q_{inv} is an integral parameter that is fully independent of the specific spatial arrangement of particles within the sample, if both the scattering densities and the volume fractions of the particle and the medium are constant[22, 23]. For NbO$_2$OH, NbO$_2$OH/H$_2$O$_2$ and NbO$_2$OH/amp the obtained values are, respectively, 3.422, 2.580 and 2.458 a.u. Q_{inv} is proportional to the electronic density, ρ, of the samples[21, 24], thus $\rho_{NbO_2OH} < \rho_{NbO_2OH/H_2O_2} < \rho_{NbO_2OH/amp}$.

For Porod scattering regime, the high-q regime, Equation 3:

$$\lim_{q \to \infty} q^4 I_{(q)} \equiv K_p \quad \text{(eq. 3)}$$

K_p is called the Porod limit or the Porod constant, obtained by the Porod plot, Figure 6. For the sutied systems K_p of NbO$_2$OH and NbO$_2$OH/H$_2$O$_2$ is 6.8 and 4.9 for NbO$_2$OH/amp.

Equation 3 is valid for dilute solution of monodisperse particles[25]. For a non-ideal two-phase system, Figure 6, will show linear relation with a negative or a positive slope representing a negative or positive deviation from Porod's law[26]. The presence of either thermal electronic movement or compositional heterogeneity within scattering elements causes positive deviations[19], and the presence of the diffuse phase boundary results in a negative slope of Porod's plot[14].
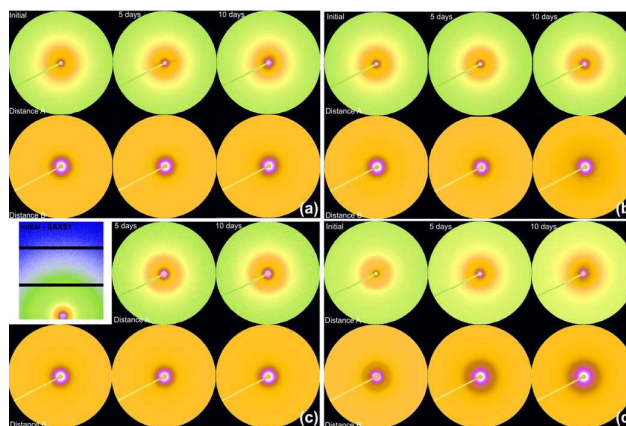
Figure 7 – SAXS patterns: (a) PP, (b) PP/NbO$_2$OH, (c) PP/NbO$_2$OH/H$_2$O$_2$ and (d) PP/NbO$_2$OH/amp.

The minor positive and the negative deviation coexist in NbO$_2$OH, Figure (a). The reason for the positive deviation is the distorted structure of atoms irregularly distributed around the Nb atoms[17], which results in fluctuation of electron density. Besides, negative deviation suggests a diffuse boundary. The interphase thickness, σ, can be estimated from $[(-slope)/4\pi^2]^{1/2}$. The σ of NbO$_2$OH is 0.06. On the other hand, NbO$_2$OH/amp σ is 0.23.

The negative deviation is not observed at NbO$_2$OH/H$_2$O$_2$, apparently, the compact boundary is the result of the hydrogen bonds between the hydrogen atoms of the hydroxyl groups and oxygen atoms. On the other hand, the Porod´s plot of NbO$_2$OH/amp presented at Figure (b) shows more complex information, suggesting that the hybrid system has significantly different surface composition.

At Figure 6(b), the strong negative deviation is due to the diffuse-boundary and due the electrostatic interaction between the surfactant organic molecular chains and Nb=O, Nb–O or Nb(O–O) groups which leads the interfaces to stimulate the negative deviation[17].

3.2.2-The macromolecular structure of pure PP and PP/Nb composites

As a semi-crystalline polymer, PP contains crystalline lamellae due to chain folding. Although a PP complex and multifaceted crystalline architecture was exhibited to the lamellar (nanoscale) and macroscopic level (micron scale), the SAXS technique is only efficient for determining the structure (i.e., average values of structure parameters) of the fine structures at the nanometer level. Figure 7 presents the SAXS patterns of pure PP and PP/Nb nanocomposite before and after photo-degradation.

Figure 7, the patterns and intensity are dependent on the shape, size and distribution of scattering objects, and the scattering arises from the 'the three-phase system' built by the crystalline, the amorphous matrix and the particles. It has been assumed that the observed SAXS pattern corresponds to the scattering of αPP, which is the most widely occurring crystal structure of PP[15].
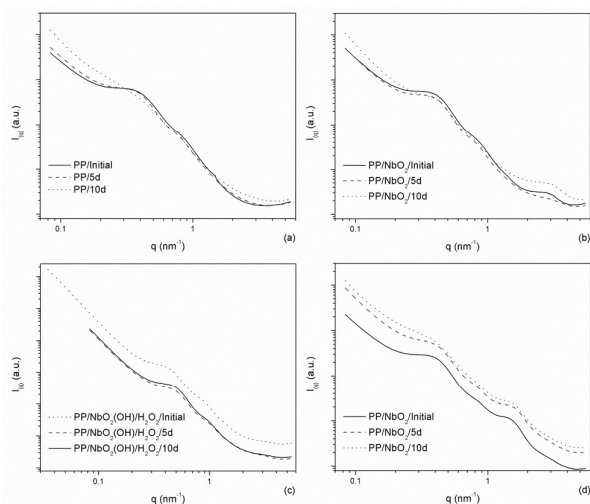
Figure 8 – SAXS curves of: (a) PP, (b) PP/NbO$_2$OH, (c) PP/NbO$_2$OH/H$_2$O$_2$ and (d) PP/NbO$_2$OH/amp.

Figure 9 – Lorentz corrected plot of: (a) PP, (b) PP/NbO$_2$OH, (c) PP/NbO$_2$OH/H$_2$O$_2$ and (d) PP/NbO$_2$OH/amp.

The additives introduced in the matrix modify the structural parameters of the crystals (i.e., size, shape, surface) instead of their type of packing. The SAXS pattern in Figure 7 displays primarily random distributions of nanostructures in the amorphous polymer matrix.

Figure 8 presents the scattering intensity, $I_{(g)}$, as a function of the scattering vector q.

The lamellar structure of pure PP and PP/Nb nanocomposites originates a peak around $q_1 = 0.4$ nm^{-1} and a bump next to $q_2 = 0.8$ nm^{-1}. The peak position of the PP/Nb nanocomposite, in respect to pure PP, slightly shifts to higher q values, which suggests an decrease in the spacing of the periodical lamellar structure and a higher degree of order [21]. Pure PP peak position and peak intensity are more affected by photo-degradation than PP/Nb nanocomposite, suggesting that the nanoparticles interfere in the degradation process. NbO$_2$OH/H$_2$O$_2$ specimen was investigated with the 3 stacked modules detector which explains the higher scattering intensity and the data $q < 0.8$ nm^{-1}.

Figure 9 shows the Lorentz corrected plot of PP and its nanocomposites. To improve visualization, the degraded curves were shifted along the y-axis. The calculation was performed for the not shifted curves.

In Figure 9 the scattering caused by lamellae in matrix is represented by a numerical index and nanoparticle scattering peaks is represented by a letter. In **Error! Reference source not found.**(a), every profile shows a very well defined peak at q_1 and a broad peak at q_2. Additonally, before degradation, the PP specimen shows a much weaker peak at q_3 which is less visible for PP/Nb nanocomposites and it is not present at PP degradaded specimen. These maximums can be accepted as first- second-and third-order Bragg reflections of a reciprocal lattice. After 10 days of photo degradation, pure PP shows a small shoulder at q_4, the shoulder indicate the βPP presence. The shape of PP/Nb nanocomposite plots is the superimposed on the scattering caused by reciprocal lattice of PP and the scattering caused by the Nb nanoparticle.
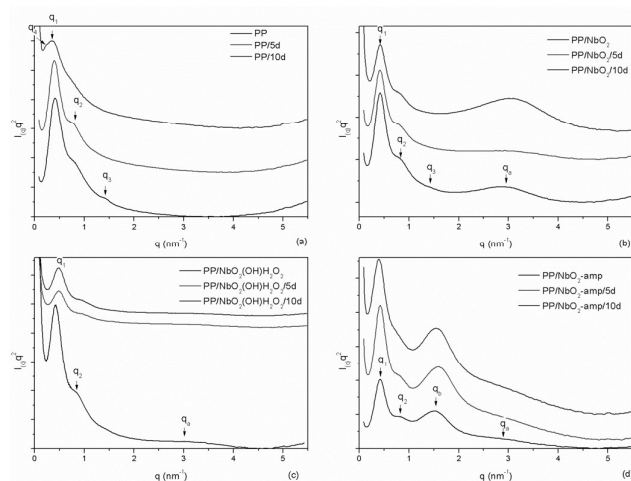
The microstructural periodicity may be obtained from unoriented SAXS patterns assuming the system is globally isotropic but locally lamellar, which is correct for undeformed samples. The inter-domain repeat distance, L, can be estimated, according to Bragg's law, from q_{max}, which corresponds to the maximum of the first peak (Equation 4).

$$L = \frac{2\pi}{q_{max}} \text{ (eq. 4)}$$

The integrated scattering intensity, Q_{inv}, Equation 1, was obtained for all specimens. It provides an estimation of the degree of phase separation and it is proportional to the phase electron density and to the phase volume fraction [23].

We are aware of the fact that the use of this correction for semicrystalline polymers reinforced by nanoparticles may be criticized because it might produce an artificial peak and the different phases scattering will be superimposed. As observed in Figure 9 (b-d), the nanoparticle presence affects the shape of the curve, such that invariant Q_{inv} could not be used for calculations. Nevertheless, in order to obtain information on the overall difference in electron density of the samples, the PP contribution and the nanoparticle contribution to Q_{inv} were calculated. The contribution of each phase were separated according to a deconvolution procedure[2], Figure 11. Because the scattering from the different phases has been separated, further analysis of data are possible [26, 27]. The Table 1 presents the results. At Table 1, the equidistant peaks indicate the presence of lamellar structures in the samples (for lamellar morphology, the q value of the Bragg's show relationships 1:2:3:4:5)[2]. After photo-degradation, the peak position of the PP shifts to lower q values, indicating the degradation, i.e. lower degree of order, of the periodical lamellar structure. The PP/nanocomposites present a different behavior. The peak position of PP/NbO$_2$OH is hardly affect by degradation, so the periodical lamellar structure is kept constant during the process.
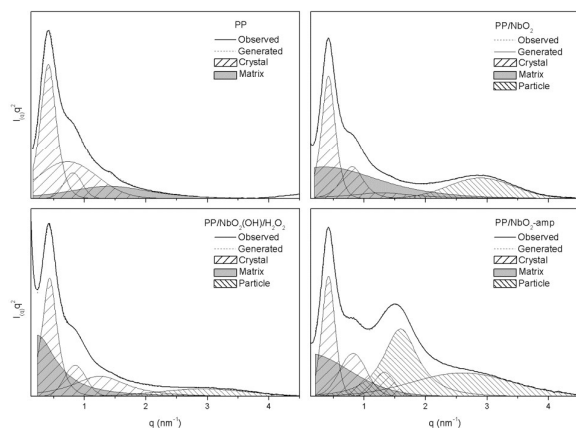
Figure 10 – Deconvoluted Lorentz plot before photo-degradation.
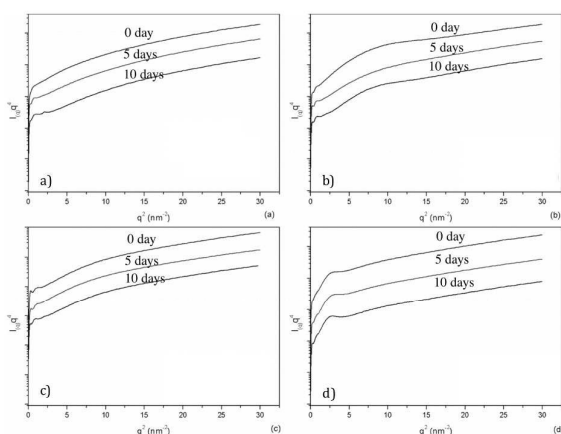
Figure 11 – Porod's plot of: (a) PP, (b) PP/NbO2, (c) PP/NbO2(OH)/H2O2 and (d) PP/NbO2/amp.

Moreover, PP/NbO$_2$OH $Q_{Particle}^{inv}$ results suggest that the phase separation increases because the particle contribution to the scattering intensity rises. These results can be explained by the larger size of the inorganic phase, as shown in the SEM results. The βPP is not detected at PP/NbO$_2$OH until 10 days. However, $Q_{crystal}^{inv}$ suggests the crystal turn into a less compact structure. PP/NbO$_2$OH/H$_2$O$_2$ results suggest a opposite behavior. The phase separation decreases because the matrix contribution to the scattering intensity rises. During photo degradation, the peak position of the PP/NbO$_2$OH/H$_2$O$_2$ slightly shifts to higher q values and $Q_{crystal}^{inv}$ $Q_{Crystal}^{inv}$ decreases thus results can not be interpreted as a higher degree of order but a crystal distortion. Finally, the phase separation and the periodical lamellar structure PP/NbO$_2$OH/amp is not affected by after 5 days of photo-degradation, the parameters obtained to the sample after 5 days until 10 days is very similar. Figure 11 presents Porod's plot of all studied specimen. In order to improve visualization, data were shifted along the y-axis. All specimen present a positive deviation of Porod's law and, therefore, compositional heterogeneity and a sharp interface. As observed, the specimen that presents the most significant differences after photo-degradation is the PP/10 days.
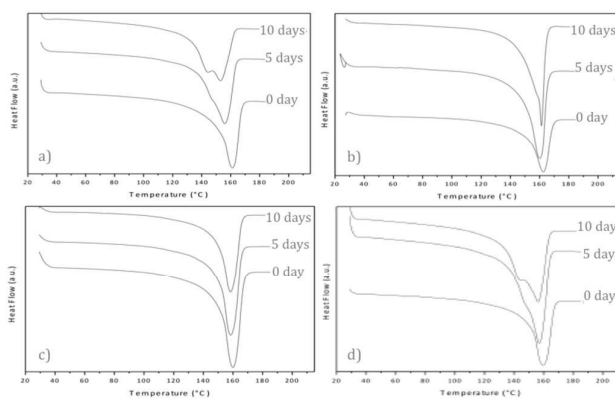
Figure 12 - DSC curves of pure PP (a) and PP/niobium composite materials: PP/NbO$_2$OH (b), NbO$_2$OH/H$_2$O$_2$ (c) and NbO$_2$OH/amp (d) unexposed and after 5 and 10 days exposure.

The crystalline structure of the PP and PP/Nb compounds that were unexposed and exposed to UV radiation was investigated by DSC analysis (Figure 12). The DSC curves shown are second run which are similar to the first run curves. The unexposed pure PP and the PP/Nb compounds exhibited a single endothermic peak with a maximum at approximately 160°C due to PP melting. However, the DSC profile curves of the UV irradiated samples after 5 and 10 days differ from that of pure PP. These curves were dependent on the added niobium compound, with the exception of the PP/NbO$_2$OH/amp. A peak with a slight shoulder (double peak) at a low temperature was obtained for all samples after 5 days of exposure becomes more obvious after a longer time (10 days) with the exception of the PP/NbO$_2$OH/H$_2$O$_2$. However, this shoulder is less apparent to PP/NbO$_2$OH than pure PP. The double peak in the DSC curves of PP was due to the presence of a significant amount of β-phase.

Under standard conditions, polypropylene preferentially crystallizes into the monoclinic α-phase. However, during crystallization of pure PP from melt, the formation of a minute amount of trigonal β-phase is typically observed[28]. The α-phase melt appears at a higher temperature than the β-phase. Therefore, the double peak in the DSC curves is due to the coexistence of two phases. However, the absence of a lower temperature peak does not imply the absence of the β-phase in the PP because the β-phase is thermodynamically unstable resulting in recrystallization into α-phase during heating in the DSC cell. The β→α recrystallization is gradually suppressed upon UV exposure[28], which may be due to chain scission and introduction of defects into the crystalline phase. Therefore, the double peak was observed in the DSC curve. In all cases, the presence of NbO$_2$OH/H$_2$O$_2$ and NbO$_2$OHin PP appears to inhibit the appearance of the double peak after UV exposure. This effect is most pronounced in PP/NbO$_2$OH/H$_2$O$_2$. In addition, this effect was also observed for the PP containing NbO$_2$OH after 10 days of exposure but to a lesser extent. The NbO$_2$OH/amp has a behavior that is closer to the pure PP.

Advanced Materials

ARTICLE

Table 1 – Peak position of PP and PP/Nb nanocomposite before and after photo-degradation.

nm^{-1}	PP			PP/NbO$_2$OH			PP/NbO$_2$OH/H$_2$O$_2$			PP/NbO$_2$OH/amp		
	0 d	5 d	10 d	0 d	5 d	10 d	0 d	5 d	10 d	0 d	5 d	10 d
q_1	0.412	0.399	0.341	0.419	0.412	0.419	0.433	0.488	0.490	0.419	0.419	0.387
q_2	0.812	0.812	0.812	0.851	0.851	0.851	0.850	0.980	0.980	0.825	0.812	0.812
q_3	1.431	-	-	-	-	-	-	-	-	-	-	-
q_4	-	-	0.238	-	-	-	-	-	-	-	-	-
q_1	-	-	-	2.950	3.084	3.106	2.950	3.084	3.039	2.950	3.084	3.084
q_1	-	-	-	-	-	-	-	-	-	1.498	1.588	1.543
L (nm)	15.24	15.73	18.40	15.00	15.24	15.00	14.51	12.89	12.83	15.00	15.00	16.25
Q_{inv}	6.22	5.74	6.21	6.63	5.20	9.04	4.99	10.79	13.18	20.98	6.41	7.07
Crystal (%)	65.8	68.9	27.9	45.8	45.9	30.5	61.3	58.8	59.7	32.2	31.4	31.4
Particle (%)	0.0	0.0	0.0	21.1	17.3	43.4	10.9	11.4	8.5	51.4	52.8	52.8
Matrix (%)	34.2	31.1	72.1	33.1	36.8	26.0	27.8	29.7	31.8	16.4	15.8	15.8
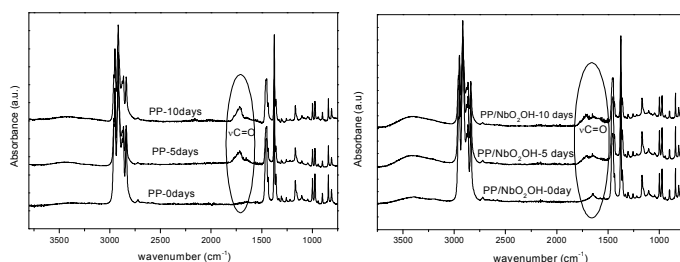
Figure 13- FTIR spectra PP and PP/NbO$_2$OH before and after 5 and 10 days irraditation UV

To investigate the extent scission chains by exposing the sample surface to UV radiation, the formation of carbonyl groups was studied using ATR infrared spectroscopy. The FTIR-ATR technique provides surface characterization and is sensitive to approximately a few microns into the surface of the samples. According to Zhao[12], the extent of degradation process in polymer is more pronounced at the surface than in the core region. The FTIR–ATR spectra of pure PP and the PP/Nb compounds (Figure 13) were obtained and used to calculate the carbonyl index of the samples before and after UV light exposure. The hydroxyl index can also be calculated to investigate the chain photo-degradation of PP[5]. However, there are hydroxyl groups in the structure of all of the niobium compounds that could interfere in the band area at ~ 3500 cm^{-1} and influence the results invalidating this study. Carbonyl index variations calculated for all of the samples are shown in Figure 14. This index was based on the ratio of the area under the bands located at 1720 and the 1168 cm^{-1}, which are associated with the C=O stretching and vibrational mode of

CH$_3$ in the PP structure. The last one was used as a reference band because it should be mostly unaffected by photo-degradation according to the proposed mechanisms. For all of the samples, the increase in the carbonyl index from 0 to 10 days of exposure indicated that they were degraded after UV light exposure, which was different for the individual samples. Carbonyl groups were incorporated into the molecular structure of PP during photo-degradation in the presence of oxygen. A larger increase was observed for the pure PP samples compared to those of the PP/Nb compounds, which indicated that it was the most affected by UV light exposure. The carbonyl index is just relative parameter used to comparison between these samples because the FTIR/ATR is not quantitative technic. However, these results indicated that the niobium compounds may stabilize the PP structure delaying the photo-degradation. The carbonyl index is similar for the PP/NbO$_2$OH and PP/NbO$_2$OH/H$_2$O$_2$. This index to PP/NbO$_2$OH/amp is biggest of PP/Nb compounds, but shorter than pure PP. All results obtained showed that the NbO$_2$OH/amp compound, initially is not as effective to retard photo-degradation of the polymer as the others, but prevents significant change in properties after a certain aging time.

The carbonyl index reduced of ~67% to sample PP/NbO$_2$/H$_2$O$_2$ compared pure PP after 10 days of exposure UV radiation (max= 340 nm). Generally, the evolution of carbonyl band is used for a qualitative description of the extent of photo-oxidation[12] and investigation of relative photostabilization efficiency[29]. Zhao et al. [12] investigated the ZnO nanoparticles as photostabilities to PP, to nanocomposite with 1,5% wt of filler appears the reduction of ~47% of carbonyl index in

relation of unfilled PP after 12.5 days of UV radiation exposure (λmax= 340 nm) on each side. Sun *et al.*[29] studied the photostabilizing efficiency in PP of commercial HALS (Cyabsorb UV-3529) by UV radiation. Considering a time of 6 h irradiation (λmax= 310 nm), it was observed a reduction of approximately 63% of the absorbance carbonyl band after the addition of the commercial HALS compared to pure PP. Based only on the relation of carbonyl index between filler PP and unfiller PP to a different system it can be concluded that the niobium nanoparticles have a photostabilization efficiency similar to commercial HALS and better than other inorganic particles.
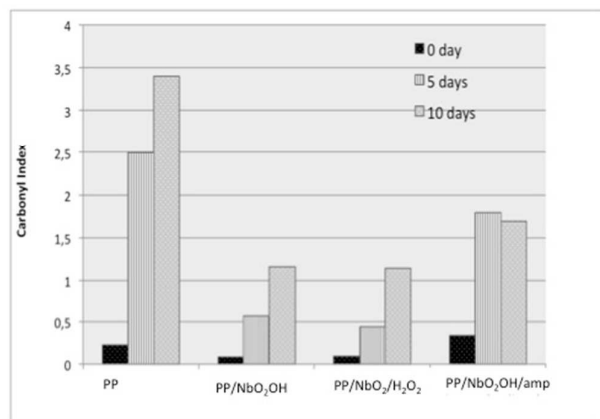
Figure 14 - Comparison between the change in the carbonyl index with the exposure time of pure PP (a) and the PP/niobium composite materials.

0 day   5 days   10 days
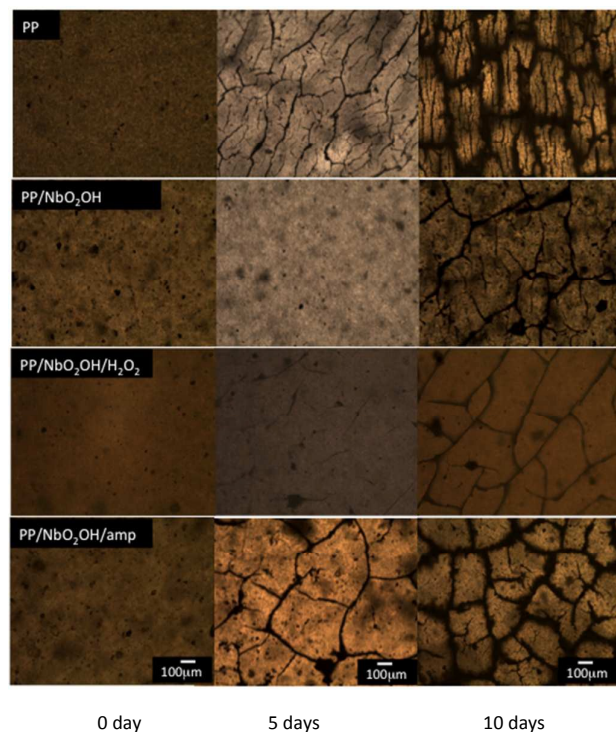
Figure 15 - Optical micrographs showing the surface cracks before and after UV irradiation.

During photo-degradation, tie chain and entanglements of PP molecules are released due to the chain scission reaction, which produces free segments in the amorphous regions that can form crystals due to increase mobility, most likely grown under pre-existing crystals. This process is called chemi-crystallization. Frequently, the extent scission chains are related to the photo-degradation process.

According to Rabello *et al.* [30], the most important result of chemi-crystallization is the spontaneous formation of surface cracks. The surface morphology of the PP/Nb compounds and pure PP was investigated by optical microscopy (OM) (Figure 15). Rosa *et al.* [31] reported that OM is a quick and simple method for monitoring the degradation of PP. The unexposed surfaces of all of the PP/Nb samples were smooth, and no cracks were observed. In comparison to all of the exposed samples after 5 days, the surface cracks caused by UV irradiation appear in pure PP and PP/NbO$_2$OH/amp, which is in contrast to PP/NbO$_2$OH/H$_2$O$_2$ and PP/NbO$_2$OH.
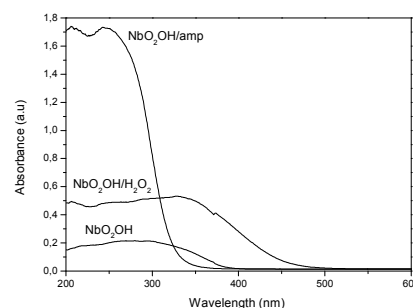
Figure 16- UV-Vis absorbance spectra obtained via the diffuse reflectance method

However, there are cracks in all of the samples after 10 days of exposure to UV light, but with a different quantity, thickness and depth. The cracks on the surface of PP/NbO$_2$OH/H$_2$O$_2$ are the thinnest. The surface profile measurements indicate that the severity of the surface cracks was reduced after the addition of the Nb compounds in the following order: PP/NbO$_2$OH/H$_2$O$_2$ < PP/NbO$_2$OH < PP/NbO$_2$OH/amp. The results indicate that the addition of Nb compounds to PP leads to a reduction in the extent of photo-degradation. In addition, visible changes in the polymer without the niobium compound were observed.

Finally, the materials were characterized by diffuse reflectance spectroscopy, and the results are shown in Figure 16. The results showed that the NbO$_2$OH/amp compound is highest efficient to absorbed incident radiation, followed by NbO$_2$OH/H$_2$O$_2$ and lastly NbO$_2$OH. However, it is necessary to consider that the tests under UV radiation were performed using a source with energy of 340 nm. Considering that energy and profiles of energy absorption by the materials obtained via diffuse reflactance (Fig. 16) can be seen that the NbO$_2$(OH)/H$_2$O$_2$ has higher absorption capacity in this energy. In fact, even when the PP/NbO$_2$OH/amp material has a greater

absorption capacity for higher energy wavelength in the employed energy the material $NbO_2(OH)/H_2O_2$ works best as a filter. This result indicates that process of photodegradation of the PP/niobium compounds is explained mainly by UV absorption capacity of nanoparticles. Furthemore, the size of niobium compounds into PP matrix and better dispersion of particles are additional effects that contribute to improve the ability of compounds of niobium absorb UV radiation.

4. Conclusions

The results from this research study indicate that the incorporation of niobium oxyhydroxide nanoparticles into the PP matrix provide stability against the action of ultraviolet radiation. The PP/Nb compounds are less susceptible to photo-degradation than pure PP, even with a higher content of amorphous phase, which is more susceptible to degradation. It has been demonstrated for the first time that compounds niobium modified by H_2O_2 incorporated into the PP polymer have the ability to efficiently absorb radiation and preventing radiation induced polymer degradation. The surface modifications were able to act on the ability of the compounds as PP photo-stabilizers. NbO_2OH/H_2O_2 exhibited the highest efficiency for delaying the photo-degradation process of the PP due to size compared to NbO_2OH and $PP/NbO_2OH/amp$, which resulted of UV absorption capacity and better dispersion in the polymer matrix. The SAXS technical is efficient to studied structure of nanoparticles after the superficial modifications and analyses the nanostructure polymer after photo-degradation.

Acknowledgements

Notes and references

1. Zhang, R.; Xü, Y.; Meng, Q.; Zhan, L.; Li, K.; Wu, D.; Ling, L.; Wang, J.; Zhao, H.; Dong, B. *The Journal of Supercritical Fluids* **2004,** 28, (2–3), 263-276.

2. Campos, D. D. P. d.; Cassu, S. N.; Garcia, R. B. R.; Queiroz, H. A. A. d. S.; Gonçalves, R. F. B.; Kawachi, E. Y. *Química Nova* **2012,** 35, 355-359.

3. Kumar, A. P.; Depan, D.; Singh Tomer, N.; Singh, R. P. *Progress in Polymer Science* **2009,** 34, (6), 479-515.

4. Rivaton, A.; Serre, F.; Gardette, J. L. *Polymer Degradation and Stability* **1998,** 62, (1), 127-143.

5. Waldman, W. R.; De Paoli, M. A. *Polymer Degradation and Stability* **1998,** 60, (2–3), 301-308.

6. Wiles, D. M.; Carlsson, D. J. *Polymer Degradation and Stability* **1980,** 3, (1), 61-72.

7. George, G. A.; Ghaemy, M. *Polymer Degradation and Stability* **1991,** 33, (3), 411-428.

8. Gugumus, F. *Polymer Degradation and Stability* **1991,** 34, (1–3), 205-241.

9. Li, J.; Yang, R.; Yu, J.; Liu, Y. *Polymer Degradation and Stability* **2008,** 93, (1), 84-89.

10. Qin, H.; Zhang, S.; Liu, H.; Xie, S.; Yang, M.; Shen, D. *Polymer* **2005,** 46, (9), 3149-3156.

11. Esthappan, S. K.; Kuttappan, S. K.; Joseph, R. *Polymer Degradation and Stability* **2012,** 97, (4), 615-620.

12. Zhao, H.; Li, R. K. Y. *Polymer* **2006,** 47, (9), 3207-3217.

13. Ammala, A.; Hill, A. J.; Meakin, P.; Pas, S. J.; Turney, T. W. *Journal of Nanoparticle Research* **2002,** 4, (1-2), 167-174.

14. Oliveira, L. C. A.; Oliveira, H. S.; Mayrink, G.; Mansur, H. S.; Mansur, A. A. P.; Moreira, R. L. *Applied Catalysis B: Environmental* **2014,** 152–153, 403-412.

15. Nogueira, A.; Ramalho, T.; Oliveira, L. A. *Top Catal* **2011,** 54, (1-4), 270-276.

16. Oliveira, L. C. A.; Portilho, M. F.; Silva, A. C.; Taroco, H. A.; Souza, P. P. *Applied Catalysis B: Environmental* **2012,** 117–118, (0), 29-35.

17. de Oliveira, L. C. A.; Costa, N. T.; Pliego Jr, J. R.; Silva, A. C.; de Souza, P. P.; de O. Patrício, P. S. *Applied Catalysis B: Environmental* **2014,** 147, (0), 43-48.

18. di Stasio, S.; Mitchell, J. B. A.; LeGarrec, J. L.; Biennier, L.; Wulff, M. *Carbon* **2006,** 44, (7), 1267-1279.

19. Pereira, I. M.; Oréfice, R. L. *Polymer* **2010,** 51, (8), 1744-1751.

20. Pereira, I. M.; Oréfice, R. L. *J Mater Sci* **2010,** 45, (2), 511-522.

21. Skrzypek, J.; Ganczarski, A. W.; Rustichelli, F.; Egner, H., *Advanced Materials and Structures for Extreme Operating Conditions*. Springer: Germany, 2008.

22. Bolze, J. P., D; Ballauff, M; Narayanan, T; Cölfen H. *Journal of Colloid and Interface Science* **2004,** 277, (1), 84-94.

23. Xie, R.; Yang, B.; Jiang, B. *Physical Review B* **1994,** 50, (6), 3636-3644.

24. Luo, J.; Liang, Y.; Yang, J.; Niu, H.; Dong, J.-Y.; Han, C. C. *Polymer* **2011,** 52, (20), 4590-4599.

25. Vainio, U.; Lauten, R. A.; Serimaa, R. *Langmuir* **2008,** 24, (15), 7735-7743.

26. Xiao-Xu, L.; Jing-Hua, Y.; Dao-Bin, S.; Wen-Bin, B.; Wei-Dong, C.; Zhong-Hua, W. *Chinese Physics Letters* **2010,** 27, (9), 096103.

27. Cser, F.; Hopewell, J. L.; Shanks, R. A. *Journal of Applied Polymer Science* **2001,** 81, (2), 340-349.

28. Výchopňová, J.; Čermák, R.; Obadal, M.; Raab, M.; Verney, V.; Commereuc, S. *Polymer Degradation and Stability* **2007**, 92, 1763-1768.

29. Sun, G. J.; Jang, H. J.; Kaang, S.; Chae K. H. *Polymer* **2002**, 43, 5855–5863.

30. Rabello, M. S.; White, J. R. *Polymer* 1997, 38, 6379-6387.

31. Rosa, D. S. J.; Angelini, M. G.; Agnelli, J. A. M.; Mei, L. H. I. *Polymer Testing*, **2005**, 24, 1022-1026.